

# Geophysical Research Letters

## RESEARCH LETTER

10.1029/2018GL077342

### Key Points:

- A novel channel-synthesizing technique is proposed for reducing uncertainties in brightness temperature simulation
- The technique is demonstrated to be effective in both simulated and real-data experiments for GOES-R radiances
- The proposed technique will alleviate the uncertainties in surface emissivity and skin temperature that can induce both biases and noises

### Correspondence to:

F. Zhang,  
fzhang@psu.edu

### Citation:

Lu, Y., & Zhang, F. (2018). A novel channel-synthesizing method for reducing uncertainties in satellite radiative transfer modeling. *Geophysical Research Letters*, 45. <https://doi.org/10.1029/2018GL077342>

Received 29 JAN 2018

Accepted 7 APR 2018

Accepted article online 19 APR 2018

## A Novel Channel-Synthesizing Method for Reducing Uncertainties in Satellite Radiative Transfer Modeling

Yinghui Lu<sup>1</sup>  and Fuqing Zhang<sup>1</sup> 

<sup>1</sup>Department of Meteorology and Atmospheric Science and Center for Advanced Data Assimilation and Predictability Techniques, The Pennsylvania State University, University Park, PA, USA

**Abstract** Most sounding channels sensitive to atmosphere layers close to Earth's surface are also sensitive to Earth's surface properties. Biases and uncertainties in Earth's surface emissivity and skin temperature may degrade the values of these observations being assimilated into weather prediction models. A method that combines several individual channels into a synthesized channel is proposed here to reduce such uncertainties. The effectiveness of such channel-synthesizing method is first demonstrated through perfect model experiments, where brightness temperatures are simulated and compared before and after noises added to surface emissivity and skin temperature. Real-case experiments that compare simulated brightness temperature and satellite observations further show that the synthesized channel can effectively reduce the mean bias of simulated brightness temperature from 1 to 3 K for individual GOES-R channels to near zero for the synthesized channel, suggesting great potential of the approach for more effective assimilation of surface-sensitive sounding channels.

**Plain Language Summary** Satellite observation is one of the most impactful sources of observations assimilated into weather prediction models. Satellite channels sensitive to atmosphere layers close to Earth's surface are usually sensitive to the Earth's surface properties. Due to the large uncertainty in Earth's surface emissivity and skin temperature, these satellite channels are not well utilized. Here we propose a novel method that combines several individual channels into a synthesized channel to reduce the sensitivity to Earth's surface properties by calculating coefficients for each channel so that influences from Earth's surface properties cancel. For example, if the errors in calculated brightness temperature of three channels due to surface emissivity error are 5, 2, and 4 K, respectively, and errors due to skin temperature error are 4, 2, and 3.5 K, respectively, a synthesized channel equals  $2 \cdot CH_1 + 3 \cdot CH_2 - 4 \cdot CH_3$  will be used so that the errors cancel. Our real-case experiments using GOES-R observations show that this channel-synthesizing method can effectively reduce mean bias of simulated brightness temperature from 1 to 3 K for individual channels to near zero for the synthesized channel, suggesting great potential of the approach for more effective assimilation of surface-sensitive sounding channels.

### 1. Introduction

Sounding channels of satellite-based passive radiometer observations provide rich information content in the vertical profiles of atmospheric temperature and humidity (Menzel et al., 2018). They are shown to be impactful in reducing the forecast error (Joo et al., 2013; Zhang et al., 2016; Zhu et al., 2012). Their sensitivity on Earth's surface properties, that is, surface emissivity and skin temperature, is determined by surface-to-space transmissivity (English, 2008). Channels with frequencies away from strong absorptions of atmosphere constitutes have large space-to-surface transmissivity and are informative of temperature and humidity close to the Earth's surface and Earth's surface properties. Such information is valuable for data assimilation and weather forecast. Gartzke et al. (2017) show that temperature and humidity at the surface layer are crucial for convective available potential energy, which is a widely used parameter for convection study. However, due to the uncertainties in surface emissivity and skin temperature over land, these surface-sensitive channels are not well utilized over land in data assimilation (Pavelin & Candy, 2014).

Land surface emissivity varies with frequency and land surface properties, such as land surface type, soil moisture, vegetation, and snow cover. Various efforts have been made to obtain more accurate surface emissivity data that can be used in radiative transfer calculations. Taking infrared frequencies as an example, emissivity of various materials are measured in laboratory and composed into spectral databases, such as the

ECOSTRESS spectral library (<https://speclib.jpl.nasa.gov>, formally ASTER spectral library; Baldridge et al., 2009) and the Moderate Resolution Imaging Spectroradiometer University of California, Santa Barbara Emissivity Library (<https://icess.eri.ucsb.edu/modis/EMIS/html/em.html>). These spectral libraries are used to develop classification-based emissivity models (Peres & DaCamara, 2005; Snyder et al., 1998). The Community Radiative Transfer Model (CRTM; Han et al., 2006) follows this approach. It originally uses the National Polar-orbiting Operational Environmental Satellite System emissivity model, and another two emissivity models were developed for International Geosphere-Biosphere Programme classification and U.S. Geological Survey classification later (Han et al., 2006). As is illustrated by Seemann et al. (2008, their Figure 1), surface emissivity of different land surface types varies by 0.05 in value for 11–14  $\mu\text{m}$  wavelengths and varies by over 0.2 in value for 8–10  $\mu\text{m}$  wavelengths. As such, error in land surface classification in numerical weather prediction model can lead to large error in estimated land surface emissivity. Alternatively, surface emissivity can be estimated through satellite observations (J. Li et al., 2011; Z. Li et al., 2010). The University of Wisconsin Baseline Fit Emissivity Database is derived using input from the Moderate Resolution Imaging Spectroradiometer operational land surface emissivity product (MOD11) and a baseline fit method based on laboratory measurements (Seemann et al., 2008). This database is used in the development of the University of Wisconsin Global Infrared Land Surface Emissivity (UWiremis) module for the Radiative Transfer for the TIROS Operational Vertical Sounder (RTTOV; Matricardi et al., 2004; Saunders et al., 1999), where emissivity is a function of frequency, latitude, longitude, and month of the year. However, these emissivity models still cannot capture variations in land surface emissivity with short time scale, such as variations in surface emissivity due to soil water content change (Z. Li et al., 2012; Mira et al., 2007). These uncertainties may lead to large uncertainty in the calculated brightness temperatures. J. Li et al. (2007) show that uncertainty of 0.01 in surface emissivity value can cause about 0.5 K uncertainty in simulated brightness temperature in infrared window channels. Zou et al. (2016) also show that large differences of more than 0.03–0.06 between the surface emissivity estimated by surface emissivity lookup tables used in the CRTM and RTTOV are found over mainland Australia (their Figure 9), leading to over 2 degrees difference in simulated brightness temperatures (their Figure 10) in channel 11 of the Advanced Himawari Imager (ABI) on board the Japanese satellite *Himawari-8* (Bessho et al., 2016).

On the other hand, surface skin temperature produced by weather forecast models can have large uncertainties and biases, especially arid regions during daytime. Trigo et al. (2015) show that the land skin temperature is slightly overestimated during nighttime and seriously underestimated during daytime by the analysis of European Center for Medium-Range Weather Forecasts (ECMWF). Uncertainties in skin temperature may have larger impact on brightness temperature than uncertainties in surface emissivity over land (English, 2008). Large bias in land skin temperature over desert and arid region during daytime in the warm season causes the rejection of large amount of satellite data in the analysis step (Zheng et al., 2012). As such, uncertainties and biases in both surface emissivity and skin temperature need to be reduced before assimilating surface-sensitive satellite channels.

Surface snow water equivalent have been retrieved from satellite passive microwave imagers for decades, empirically derived from the difference in brightness temperatures between two microwave channels at which snow layers have very different scattering properties (Clifford, 2010; Xue & Forman, 2017). The advantage of this approach is that when the surface emissivity is biased toward the same direction for both channels (skin temperature is of course bias toward the same direction), the biases at the two different channels cancel and the resulting channel difference would be less sensitive to the biases and uncertainties in the estimation of surface emissivity and skin temperature. Inspired by this approach, we propose a method that combines several individual channels into a synthesized (or composite) channel, where the coefficients of the individual channels are carefully chosen so that the resulting synthesized channel is less sensitive to uncertainties in land surface properties and is more suitable to be used in the data assimilation system than the individual channels.

## 2. Methodology

In this work, the infrared imaging channels 13, 14, and 15 on the Advanced Baseline Imager (ABI) onboard the Geostationary Operational Environmental Satellite (GOES)-R (now in operational mode as GOES-16; Schmit et al., 2005, 2017) are used to illustrate the applicability of the proposed channel-synthesizing method. At

these wavelengths, contribution from the Sun can be ignored. Under clear-sky condition, a simplified emission model provides the essence of the radiative transfer process where the top of atmosphere (TOA) radiance can be calculated as the sum of three major contributors: (1) Earth's surface thermal emission that reaches TOA, (2) atmosphere downward thermal emission reflected by Earth's surface and reaches TOA, and (3) atmosphere upward thermal emission:

$$I_{\text{TOA}}(\nu) = t(\nu)\epsilon(\nu)B(\nu, T_s) + t(\nu)(1 - \epsilon(\nu))I_{\text{atm}}^{\downarrow}(\nu) + I_{\text{atm}}^{\uparrow}(\nu), \quad (1)$$

where  $t(\nu)$  is the atmosphere transmissivity,  $\epsilon(\nu)$  is the surface emissivity,  $B(\nu, T_s)$  is the surface Planck radiance,  $(1 - \epsilon(\nu))$  is the surface reflectivity,  $I_{\text{atm}}^{\downarrow}(\nu)$  is the downward radiance at the Earth's surface emitted by the atmosphere, and  $I_{\text{atm}}^{\uparrow}(\nu)$  is the upward radiance at TOA emitted by the atmosphere.

To show the impact of uncertainties in surface emissivity and skin temperature on TOA brightness temperature, equation (1) is reordered and written in a tangent linear form, such that the deviation of TOA radiance is expressed as a function of the deviations of surface emissivity and skin temperature:

$$\Delta I(\nu) = t(\nu) \left[ B(\nu, T_s) - I_{\text{atm}}^{\downarrow}(\nu) \right] \Delta \epsilon(\nu) + t(\nu)\epsilon(\nu) \left. \frac{\partial B(\nu, T)}{\partial T} \right|_{T=T_s} \Delta T_s. \quad (2)$$

Using the tangent linear form of the Planck function, where

$$\Delta T_B(\nu) = \Delta I(\nu) / \left( \left. \frac{\partial B(\nu, T)}{\partial T} \right|_{T=T_B} \right), \quad (3)$$

and define

$$M(\nu) \equiv t(\nu) \left[ B(\nu, T_s) - I_{\text{atm}}^{\downarrow}(\nu) \right] / \left( \left. \frac{\partial B(\nu, T)}{\partial T} \right|_{T=T_B} \right),$$

and

$$N(\nu) \equiv t(\nu) \epsilon(\nu) \left. \frac{\partial B(\nu, T)}{\partial T} \right|_{T=T_s} / \left( \left. \frac{\partial B(\nu, T)}{\partial T} \right|_{T=T_B} \right), \quad (4)$$

the deviation of TOA brightness temperature can be expressed as a linear combination of the deviations of surface emissivity and skin temperature, with coefficients determined by the first guess of surface properties and atmosphere profile

$$\Delta T_B(\nu) = M(\nu)\Delta \epsilon(\nu) + N(\nu)\Delta T_s. \quad (5)$$

Similar expressions have been derived in previous research (English, 2008; J. Li et al., 2000). Skin temperature that determines the surface thermal emission is difficult to define exactly, because the layers near land and ocean surface may be highly heterogeneous, which may also have complex and variable temperature structures, and the thickness into the Earth skin that contribute the most to the surface leaving radiation can be different for different frequencies (Donlon et al., 2007). Nevertheless, for the same instrument,  $\Delta T_s$  is likely to be the same for all the channels. Over ocean, uncertainties in the estimation of surface emissivity  $\Delta \epsilon(\nu)$  because of uncertainties in surface wind speed tend to be similar for infrared channels with wavelengths between 8.3 and 12.5  $\mu\text{m}$  (Wu & Smith, 1997). Over land,  $\Delta \epsilon(\nu)$  can have different values for the three channels because the relationship between emissivity and wavelength for various types of materials can have large variability (Salisbury & D'Aria, 1992). For a total of  $N$  channels, equation (5) has  $N$  equations with  $N + 1$  unknowns. To reduce the number of unknowns, we assume that  $\Delta \epsilon(\nu)$  can be modeled as

$$\Delta \epsilon(\nu_i) = C(\nu_i)\Delta \epsilon_0, \quad (6)$$

where  $C(\nu_i)$ ,  $i = 1, 2, 3$  are empirically determined. This assumption can be valid for many situations, for example, in the situation that the Earth's surface within one satellite footprint or model grid box contains two surface types, and the resulting total emissivity is a linear combination of the two. Given the assumption in equation (6), equation (2) has two unknown properties  $\Delta \epsilon_0$  and  $\Delta T_s$ .

A synthesized channel can be created as a linear combination of three channels:

$$T_B^{\text{syn}} = \sum_{i=1}^3 a_i T_B(v_i) = \left[ \sum_{i=1}^3 a_i C(v_i) M(v_i) \right] \Delta \epsilon_0 + \left[ \sum_{i=1}^3 a_i N(v_i) \right] \Delta T_s. \quad (7)$$

If the three coefficients  $a_i$  ( $i = 1, 2, 3$ ) are chosen in a way that the coefficients of  $\Delta \epsilon_0$  and  $\Delta T_s$  are zero or close to zero, the bias of the synthesized channel due to biases and uncertainties in estimation of surface emissivity and skin temperature can be reduced.

The most straightforward way to find the coefficients  $a_i$  for the synthesized channel is to solve the following set of linear equations:

$$\sum_{i=1}^3 a_i = 1, \quad (8.1)$$

$$\sum_{i=1}^3 a_i N(v_i) = 0, \quad (8.2)$$

$$\sum_{i=1}^3 a_i C(v_i) M(v_i) = 0, \quad (8.3)$$

where equation (8.1) is introduced so that the resulting synthesized channel brightness temperature would be close to that of the three channels. However, for channels with high surface-to-space transmissivity (or optical depth is small), solving equations (8.1)–(8.3) can lead to unstable results with very large coefficients. As equation (6) is not a perfect estimation, these unreasonably large coefficients can result in large bias in the resulting synthesized channel brightness temperature. Instead, we replace equation (8.3) by minimizing a cost function

$$J = W \left[ \sum_{i=1}^3 a_i C(v_i) M(v_i) \right]^2 + \sum_{i=1}^3 [a_i C(v_i) M(v_i)]^2. \quad (8.4)$$

The first term in equation (8.4) is the square of the left-hand side of equation (8.3), which relates to the error of the synthesized channel if equation (6) is perfect. The second term prevents the value of each coefficient from being too large. When  $W$  reaches infinity, minimizing the cost function defined by equation (8.4) is equivalent to solving equation (8.3). When the atmosphere optical depth is higher (transmissivity is lower), solving equations (8.1)–(8.3) would be more likely to give stable result, and thus,  $W$  can be assigned larger values indicating more weight on the first term of equation (8.4). In this study,  $W$  value is heuristically set to 100 times the total optical depth (which is much smaller than 1). It should be noted that the coefficients are calculated separately for each profile by minimizing the cost function in equation (8.4) under the constraints given by equations (8.1) and (8.2). As such, different model grids have different sets of coefficients depending on their surface properties and atmosphere profiles.

### 3. Perfect Model Experiments

Perfect model experiments are performed to test the performance of the channel-synthesizing method. In this experiment, the atmosphere profile and surface properties from the 27-km domain of the Weather Research and Forecasting (WRF; Skamarock et al., 2008) model forecast output valid at 18:00 UTC on 23 August 2017 for Hurricane Harvey (2017) (Lu & Zhang, 2018) are considered “truth.” This work emphasizes on clear-sky condition. As such, we remove all the hydrometers in the WRF output but leave the humidity profile unmodified, so that the entire model domain is pseudo-clear. GOES-R channels 13 (CH13), CH14, and CH15 brightness temperatures are calculated using CRTM (version 2.3.0) as the “observations.” Then random biases are added to surface emissivity and skin temperature fields, while the atmosphere profiles remain unmodified. This modified state serves as the “background,” and the TOA brightness temperatures are calculated again using CRTM. The difference between brightness temperatures calculated before and after the perturbation represents the sensitivity of TOA brightness temperature on surface emissivity and skin temperature. Uncertainties added to surface skin temperature follow a uniform distribution from  $-2$  to 2 K. Uncertainties added to surface emissivity also roughly follow a uniform distribution from  $-0.02$  to 0.02.

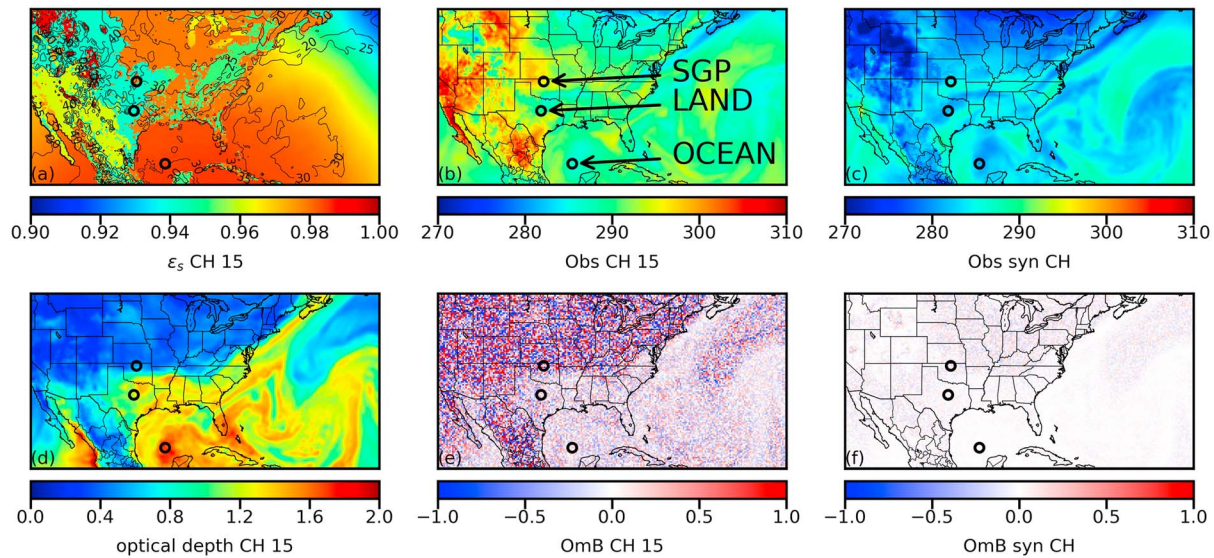


**Figure 1.** (a) Surface emissivity of GOES-R ABI CH15 (color) and skin temperature (contour); (b) observed brightness temperature at CH15; (c) observed synthesized channel brightness temperature; (d) optical depth of GOES-R ABI CH15; (e) OmB value for CH15 brightness temperature; (f) OmB value for synthesized channel. The three example locations are located at the center of the three small circles in each panel and are labeled in panel (b).

0.02, with the restriction that the resulting surface emissivity never exceeds 0.999. Same surface emissivity uncertainties are added to all the three channels for each grid point, corresponding to  $C(v_i) = 1$  in equation (6).

Figure 1a shows the surface skin temperature in the original WRF output in contours and the original surface emissivity calculated using CRTM in color. The surface emissivity used by CRTM over land is generated by a lookup table as a function of frequency and surface type, indicated by large areas of same emissivity values. Over the ocean, the ring-shaped gradual change of the emissivity is mainly caused by change in satellite zenith angle.

At the wavelengths of GOES-R CH13, CH14, and CH15, water vapor is the major absorber. The more the water vapor in the atmosphere, the larger the optical depth is. Figure 1d shows the optical depth of GOES-R CH15. Water vapor is less absorptive at CH13 and CH14 than at CH15. The optical depths at CH13 and CH14 have similar pattern as CH15 and smaller values (not shown). Brightness temperatures are larger when the surface skin temperatures are larger, the surface emissivity values are larger, and the total optical depth values of the atmosphere are smaller. Figure 1b shows the “observed” brightness temperature of CH15. Brightness temperatures of GOES-R CH13 and CH14 (not shown) have similar patterns as CH15 and larger values. Figure 1c shows the synthesized channel brightness temperature. In this case the synthesized channel brightness temperature is generally lower than that of CH15, but the difference is mostly less than 20%, so that the comparison of the biases between the synthesized channel and individual channels is meaningful.

Figure 1e shows the observation minus background (OmB) values for CH15. Despite of the randomness of the OmB values since random noises are added to the surface skin temperature and surface emissivity, the biases are generally smaller when the optical depth values are larger. This behavior is expected since less surface emitted radiance can penetrate the atmosphere and reach the satellite where the optical depth is larger; hence, less information on the surface properties can be measured by the satellite. Atmosphere optical depth at CH13 and CH14 are generally smaller than CH15, and the OmB values are generally larger in magnitude (not shown). Figure 1f shows the OmB values for the synthesized channel. Apparently, OmB values of the synthesized channel are much smaller than that of the individual channels. Given the fact that the relative differences of the synthesized channel brightness temperature and individual channels are generally less than 20%, the use of the synthesized channel does greatly reduce biases to near zero for uncertainties due to biases in the estimation of surface emissivity and skin temperature.

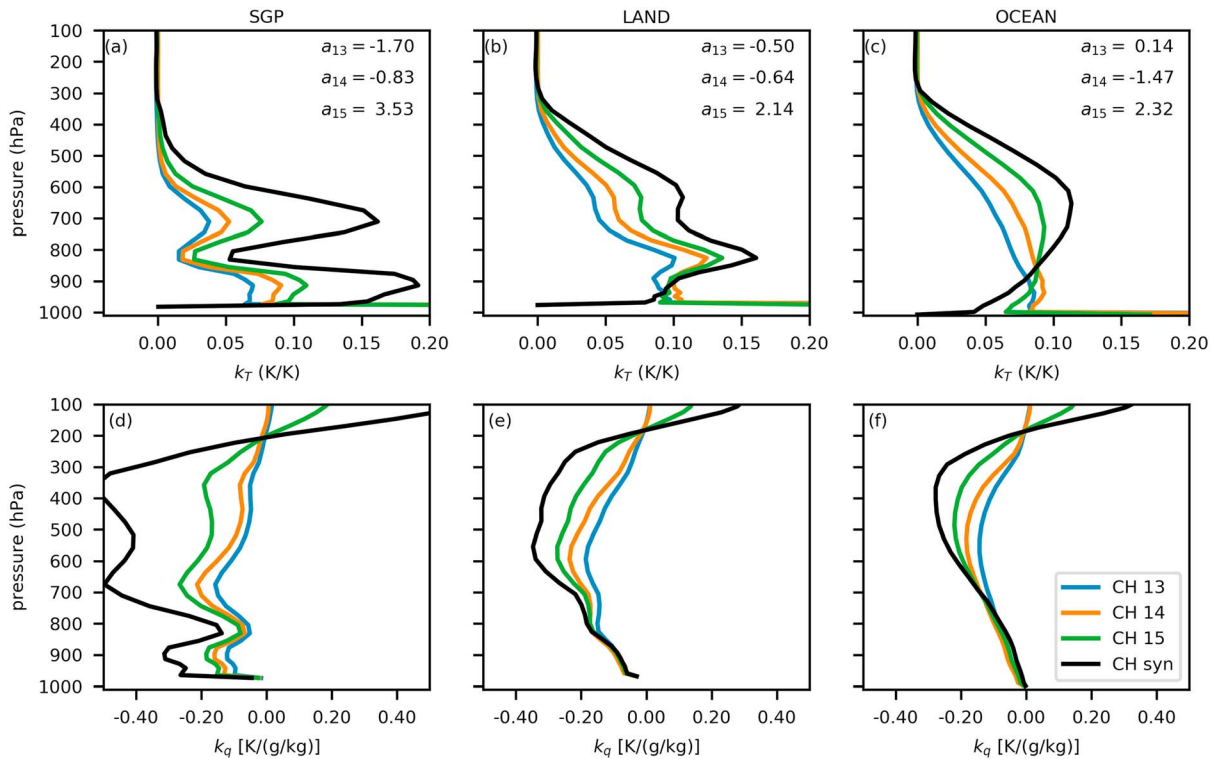


**Figure 2.** Jacobians of (a–c) temperature profile and skin temperature and of (d–f) mixing ratio profile, for example, location at ARM SGP central facility (a and d), over land (b and e), and over ocean (c and f). The coefficients that used in generating the synthesized channel are listed on the upper right corner of panels a, b, and c.

Figure 2 shows the Jacobians (the first-order partial derivatives that are closely related to weighting function) of brightness temperature against atmosphere temperature profile and surface skin temperature (Figures 2a–2c) and mixing ratio profile (Figures 2d–2f), over three example locations: Figures 2a and 2d for Atmospheric Radiation Measurement (ARM; Stokes & Schwartz, 1994) Southern Great Plains (SGP) central facility (36°36′18″N, 97°29′6″W; altitude 320 m) southeast of Lamont, Oklahoma; Figures 2b and 2e for an example over land with optical depth larger than that of ARM SGP site; and Figures 2c and 2f for an example of location with even larger optical depth value over ocean. The coefficients that used in generating the synthesized channel for each location are listed on the upper right corner of Figures 2a–2c. It should be noted that the atmosphere moisture profile was obtained from a WRF output that simply removes all the condensed hydrometers to make a pseudo-clear scene; the water vapor mixing ratio can reach water saturation where the grid boxes are originally cloudy.

Thickness of each WRF model layer can be different. For a model layer of a given temperature and humidity, the thicker in pressure coordinate (larger pressure difference between the upper and lower bound of the layer) the model layer is, the larger the response of brightness temperature to the atmosphere temperature and humidity, because more air mass is in this model layer. To make the Jacobians of different layers comparable, the Jacobians are re-scaled as if all the model layers have a thickness of 50 hPa.

Figure 2 shows that the synthesized channel generally have larger response to the atmosphere temperature and mixing ratio. Also, Figures 2a–2c show that the synthesized channel is not sensitive to the surface skin temperature (Jacobians at the bottom of the plot is zero) while the individual channels are very sensitive to the surface skin temperature (Jacobians at the bottom of the plot exceeds the axis limit and not shown). Table 1 shows surface emissivity and skin temperature Jacobians of TOA brightness temperature at the three locations for the three GOES-R ABI channels and the synthesized channel. The close-to-zero skin temperature Jacobians for the synthesized channel is expected, as equation (8.2) is used as a constraint. The surface emissivity Jacobians for the synthesized channel are smaller than any of the three GOES-R ABI channels. This shows that the synthesized channel does have a smaller sensitivity to surface properties, especially with regard to skin temperature.

**Table 1**

TOA Brightness Temperature Jacobians of Surface Temperature and Surface Emissivity for GOES-R ABI Channels 13, 14, and 15 and the Synthesized Channel

	Surface temperature Jacobian (K/K)				Surface emissivity Jacobian (K/0.01)			
	CH13	CH14	CH15	Syn CH	CH13	CH14	CH15	Syn CH
SGP	0.717	0.658	0.500	$3.70 \times 10^{-3}$	0.382	0.349	0.234	-0.112
LAND	0.493	0.384	0.230	$3.20 \times 10^{-5}$	0.210	0.151	0.074	-0.044
OCEAN	0.425	0.314	0.172	$-9.91 \times 10^{-5}$	0.139	0.088	0.036	-0.027

#### 4. Real-Data Experiments

To test the performance of the synthesized channel in more realistic scenarios, a comparison between real-data observations from GOES-R ABI and simulated brightness temperatures using CRTM over ARM SGP central facility is performed. GOES-R ABI brightness temperatures from Multi-Band Cloud & Moisture Imagery product over U.S. continent (MCMIPC) are downloaded from the Research Computing Center at the University of Chicago (<https://osdc.rcc.uchicago.edu/noaa-goes16>). Brightness temperatures of GOES-R ABI CH13, CH14, and CH15 at the satellite footprint closest to the ARM SGP site at 05:42, 11:42, 17:42, and 23:42 UTC are used as observation. Soundings are launched at the ARM SGP central facility four times per day, at roughly 05:30, 11:30, 17:30, and 23:30 UTC. Atmosphere temperature and moisture profiles ("sgpsondewnpnC1"; Atmospheric Radiation Measurement (ARM) climate research facility, 1994) from the soundings are used as input to CRTM. Trigo et al. (2015) show that "ECMWF model tends to slightly overestimate skin temperature during nighttime and underestimate daytime values." Skin temperature field from ECMWF ERA Interim reanalysis (Dee et al., 2011) at the location of ARM SGP central facility is used as input to CRTM to illustrate the influence of the potentially inaccurate skin temperature estimate to the simulated

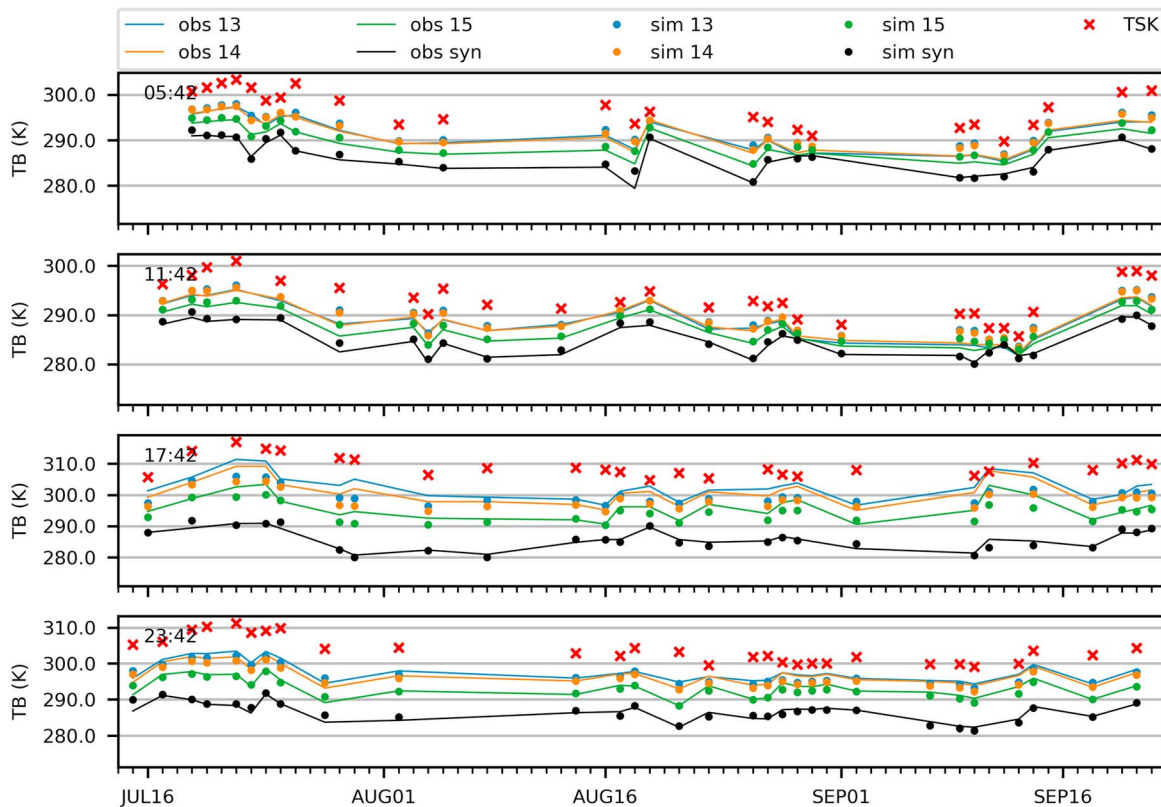


**Figure 3.** GOES-R ABI observed brightness temperatures (solid lines) and simulated brightness temperatures (dots) for GOES-R ABI CH13 (blue), CH14 (orange), CH15 (green), the synthesized channel (black), and skin temperature (red crosses), at the four sounding times at ARM SGP central facility, grouped by the time of the day. Each panel shows data at the same sounding time, with the UTC time of each sounding listed at the upper left corner of each panel.

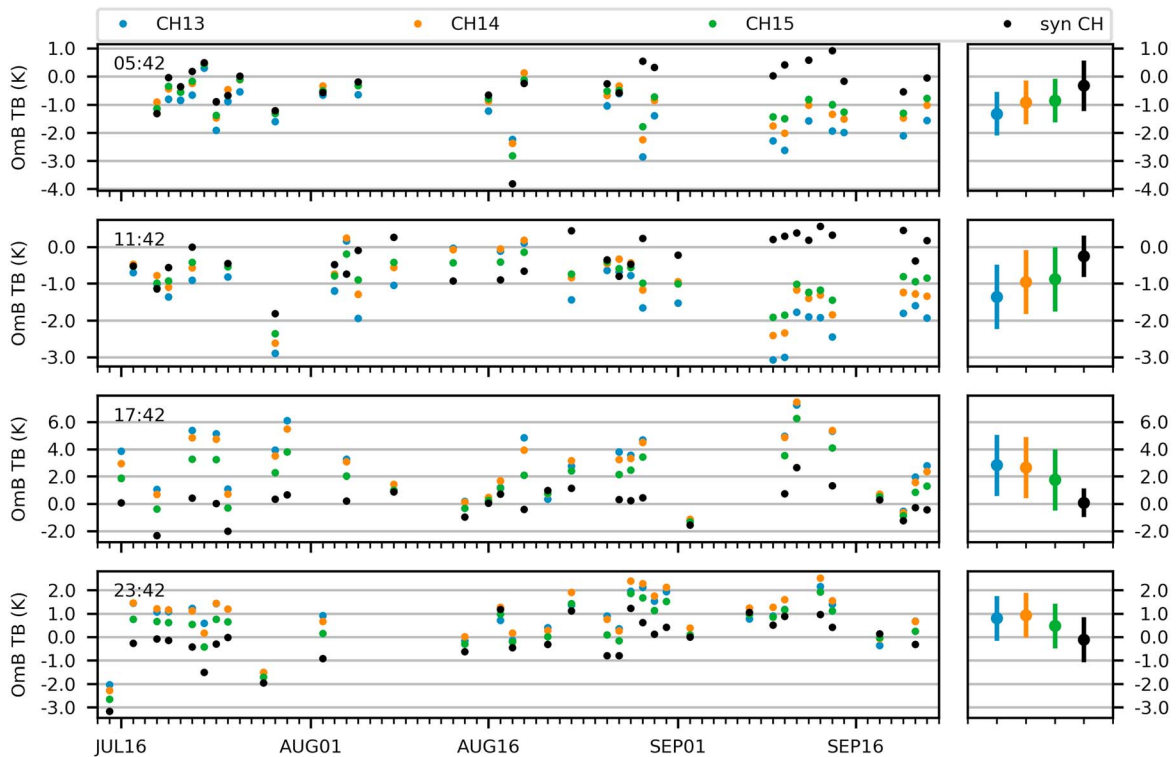


**Figure 4.** Left panels: OmB values for CH13 (blue), CH14 (orange), CH15 (green), and the synthesized channel (black) at each day. Right panels: Mean (dots)  $\pm$  standard deviation (bars) of the OmB values. UTC time of the day is shown in the upper left corner of the left panels.

brightness temperature at the three GOES-R ABI channels and the synthesized channel. Cloudy scenes are excluded based on the Micropulse Lidar 30-s cloud mask product using the first Wang and Sassen (2001) algorithm (“sgp30smplcmask1zwangC1”; Atmospheric Radiation Measurement (ARM) climate research facility, 1996) all day as well as GOES-R true-color images constructed based on GOES-R MCMIPC visible-channel data product during daytime. In this experiment, the synthesized channel is generated under the simple assumption that the biases of surface emissivity are the same for the three channels (i.e.,  $C(v_i) = 1$ ,  $i = 1, 2, 3$  in equation (6)).

Figure 3 shows the comparison of the brightness temperatures of the three individual channels and the synthesized channel, both GOES-R observation and CRTM simulation. The skin temperature given by ECMWF reanalysis is also shown for reference. ARM SGP central facility has local time about 6.5 hr later than UTC, and thus, 05:42 UTC is about local midnight, 11:42 UTC is local morning, 17:42 UTC is local noon, and 23:42 UTC is local evening. The synthesized channel has lower but comparable brightness temperature values compared to the three individual channels and is less affected by the diurnal cycle of the surface skin temperature.

The differences between simulated brightness temperatures and GOES-R observations are smaller for the synthesized channel. Figure 4 shows the differences between GOES-R observations and the simulations for easier comparison. At local midnight (05:42z) and dawn (11:42z), the OmB value is negative, indicating that the simulation is over estimating the brightness temperature, while at local noon (17:42z) and evening (23:42z) the simulation is underestimating the brightness temperature, for all the three individual channels. This agrees with the findings in Trigo et al. (2015) that ECMWF model tends to overestimates the surface skin temperature during the night and underestimates the surface skin temperature during the day. The right-hand-side plots of Figure 4 show the mean and standard deviation of the OmB bias. The largest mean bias of the three individual channels are found at local noon, where the three individual channels have mean bias of about 1.5 to 2.5 K, and standard deviation of the bias is about 3 K. The mean bias of the synthesized channel is close to zero, with a standard deviation greatly reduced to near 1 K. For the other three sounding times, the mean bias of the three

individual channels is around 1 K, and the standard deviation is about 1 K. The mean bias of the synthesized channel is still close to zero, with a standard deviation smaller than 1 K. It clearly shows that the synthesized channel has smaller mean biases with smaller error uncertainties (standard deviations) compared to the three individuals, and the synthesized channel is less affected by the diurnal cycle. It should be noted that the surface emissivity error estimate used in this test case is rather simple (i.e.,  $C(v_i) = 1$ ,  $i = 1, 2, 3$  in equation (6)). If better estimates of surface emissivity bias characteristics can be made through more sophisticated surface emissivity model, it is possible that the bias of the synthesized channel can be further reduced. Also biases and uncertainties may come from the radiometer instruments themselves.

## 5. Summary and Discussion

A novel method generating a synthesized channel not sensitive to uncertainties in surface properties using a linear combination of several individual channels is presented. Perfect-model experiments with model simulated truth observations show that the synthesized channel is less sensitive to the bias in skin temperature and surface emissivity. Real-data experiments show that even with a simplified surface emissivity bias estimation, the channel-synthesizing method can effectively reduce the mean bias of brightness temperature from 1 to 3 K for individual GOES-R channels to near zero for the synthesized channel. The standard deviation of the bias of the synthesized channel on average is usually multiple times smaller than that of individual GOES-R channels. These results suggest great potential of the proposed approach for more effective assimilation of satellite-based surface-sensitive observations into numerical prediction models: this channel-synthesizing method conceptually creates “new instruments” or “new channels” that are less sensitive to uncertainties in Earth’s surface properties, which can be used in the data assimilation system instead of assimilating the individual channels that are more uncertain. Better estimates of the surface emissivity bias characteristics may further improve the performance of the proposed method and should be investigated in the future.

This channel-synthesizing method is only tested with GOES-R ABI thermal infrared channels under clear-sky condition in this work. However, the method is not instrument specific and may also be applied to other instruments. Hyperspectral instrument such as the Infrared Atmospheric Sounding Interferometer (Clerbaux et al., 2007) has much larger number of channels that are sensitive to temperature and humidity at different layers of the atmosphere. More choices of channel combinations are available for different atmospheric conditions. For example, for dry atmosphere condition, synthesized channel can be generated using channels more sensitive to water vapor than the three GOES-R channels used in this study, such that the synthesized channel can be more sensitive to the lower level atmosphere temperature and humidity profile.

It is also possible that this method could be applied to all-sky condition after further development. Assuming that scattering is added to equation (1), it is possible that the method could be applied to microwave radiometer imaging channels over all-sky conditions. These applications are beyond the scope of this study and should be investigated in the future.

## References

- Atmospheric Radiation Measurement (ARM) climate research facility (1994). Updated daily. Balloon-borne sounding system (SONDEWNP). 2017-07-14 to 2017-09-30. Southern Great Plains (SGP) Central Facility, Lamont, OK (C1). Compiled by R Coulter, J Prell, M Ritsche, and D Holdridge. Atmospheric Radiation Measurement (ARM) Climate Research Facility Data Archive: Oak Ridge, Tennessee, USA. Data set accessed 2017-12-01 at <https://doi.org/10.5439/1021460>
- Atmospheric Radiation Measurement (ARM) climate research facility (1996). Updated daily. Cloud mask from micropulse lidar (30SMPLCMASK1ZWANG). 2017-07-14 to 2017-09-30, Southern Great Plains (SGP) Central Facility, Lamont, OK (C1). Compiled by C. Sivaraman and L. Riihimaki. Atmospheric Radiation Measurement (ARM) Climate Research Facility Data Archive: Oak Ridge, Tennessee, USA. Data set accessed 2017-12-01 at <https://doi.org/10.5439/1027736>
- Baldrige, A. M., Hook, S. J., Grove, C. I., & Rivera, G. (2009). The ASTER spectral library version 2.0. *Remote Sensing of Environment*, 113(4), 711–715. <https://doi.org/10.1016/j.rse.2008.11.007>
- Bessho, K., Date, K., Hayashi, M., Ikeda, A., Imai, T., Inoue, H., et al. (2016). An introduction to Himawari-8/9—Japan’s new-generation geostationary meteorological satellites. *Journal of the Meteorological Society of Japan, Series II*, 94(2), 151–183. <https://doi.org/10.2151/jmsj.2016-009>
- Clerbaux, C., Hadji-Lazaro, J., Turquety, S., George, M., Coheur, P.-F., Hurtmans, D., et al. (2007). The IASI/MetOp1 mission: First observations and highlights of its potential contribution to GEMS2. *Space Research Today*, 168, 19–24. [https://doi.org/10.1016/S0045-8732\(07\)80046-5](https://doi.org/10.1016/S0045-8732(07)80046-5)

### Acknowledgments

This research is partially supported by NASA grants NNX16AD84G and NNX12AJ79G and ONR grant N000140910526. ARM data were obtained from the Atmospheric Radiation Measurement (ARM) climate research facility, a U.S. Department of Energy Office of Science user facility sponsored by the Office of Biological and Environmental Research. GOES-R data set is being generously hosted by the Research Computing Center (RCC) at the University of Chicago, an OCC Member. The ECMWF model analysis is downloaded from ECMWF ERA-Interim data archive (<http://apps.ecmwf.int/datasets/data/interim-full-daily/lev-type=sfc/>). The WRF model output used in the perfect model experiment is deposited at Zenodo (<https://doi.org/10.5281/zenodo.1161807>). The authors would like to thank Masashi Minamide for providing the WRF model output used in section 3. Discussions with Eugene Clothiaux are beneficial for this study. The authors thank the two anonymous reviewers for their detailed and valuable suggestions.

- Clifford, D. (2010). Global estimates of snow water equivalent from passive microwave instruments: History, challenges and future developments. *International Journal of Remote Sensing*, 31(14), 3707–3726. <https://doi.org/10.1080/01431161.2010.483482>
- Dee, D. P., Uppala, S. M., Simmons, A. J., Berrisford, P., Poli, P., Kobayashi, S., et al. (2011). The ERA-Interim reanalysis: Configuration and performance of the data assimilation system. *Quarterly Journal of the Royal Meteorological Society*, 137(656), 553–597. <https://doi.org/10.1002/qj.828>
- Donlon, C., Robinson, I., Casey, K. S., Vazquez-Cuervo, J., Armstrong, E., Arino, O., et al. (2007). The Global Ocean Data Assimilation Experiment High-Resolution Sea Surface Temperature Pilot Project. *Bulletin of the American Meteorological Society*, 88(8), 1197–1214. <https://doi.org/10.1175/BAMS-88-8-1197>
- English, S. J. (2008). The importance of accurate skin temperature in assimilating radiances from satellite sounding instruments. *IEEE Transactions on Geoscience and Remote Sensing*, 46(2), 403–408. <https://doi.org/10.1109/TGRS.2007.902413>
- Gartzke, J., Knuteson, R., Przybyl, G., Ackerman, S., & Revercomb, H. (2017). Comparison of satellite-, model-, and radiosonde-derived convective available potential energy in the Southern Great Plains region. *Journal of Applied Meteorology and Climatology*, 56(5), 1499–1513. <https://doi.org/10.1175/JAMC-D-16-0267.1>
- Han, Y., van Delst, P., Liu, Q., Weng, F., Yan, B., Treadon, R., & Derber, J. (2006). JCSDA Community Radiative Transfer Model (CRTM) - Version 1. *NOAA Technical Report*.
- Joo, S., Eyre, J., & Marriott, R. (2013). The impact of MetOp and other satellite data within the Met Office Global NWP System using an adjoint-based sensitivity method. *Monthly Weather Review*, 141(10), 3331–3342. <https://doi.org/10.1175/MWR-D-12-00232.1>
- Li, Z., Li, J., Jin, X., Schmit, T. J., Borbas, E. E., & Goldberg, M. D. (2010). An objective methodology for infrared land surface emissivity evaluation. *Journal of Geophysical Research*, 115, D22308. <https://doi.org/10.1029/2010JD014249>
- Li, J., Li, Z., Jin, X., Schmit, T. J., Zhou, L., & Goldberg, M. D. (2011). Land surface emissivity from high temporal resolution geostationary infrared imager radiances: Methodology and simulation studies. *Journal of Geophysical Research*, 116, D01304. <https://doi.org/10.1029/2010JD014637>
- Li, Z., Li, J., Li, Y., Zhang, Y., Schmit, T. J., Zhou, L., et al. (2012). Determining diurnal variations of land surface emissivity from geostationary satellites. *Journal of Geophysical Research*, 117, D23302. <https://doi.org/10.1029/2012JD018279>
- Li, J., Li, J., Weisz, E., & Zhou, D. K. (2007). Physical retrieval of surface emissivity spectrum from hyperspectral infrared radiances. *Geophysical Research Letters*, 34, L16812. <https://doi.org/10.1029/2007GL030543>
- Li, J., Wolf, W. W., Menzel, W. P., Zhang, W., Huang, H.-L., & Achtor, T. H. (2000). Global soundings of the atmosphere from ATOVS measurements: The algorithm and validation. *Journal of Applied Meteorology*, 39(8), 1248–1268. [https://doi.org/10.1175/1520-0450\(2000\)039%3C1248:GSOTAF%3E2.0.CO;2](https://doi.org/10.1175/1520-0450(2000)039%3C1248:GSOTAF%3E2.0.CO;2)
- Lu, Y., & Zhang, F. (2018). WRF model output used in an ideal model experiment demonstrating the applicability of a channel-synthesizing method for reducing uncertainties in satellite radiative transfer modeling. Zenodo. <https://doi.org/10.5281/zenodo.1161807>
- Matricardi, M., Chevallier, F., Kelly, G., & Thépaut, J.-N. (2004). An improved general fast radiative transfer model for the assimilation of radiance observations. *Quarterly Journal of the Royal Meteorological Society*, 130(596), 153–173. <https://doi.org/10.1256/qj.02.181>
- Menzel, W. P., Schmit, T. J., Zhang, P., & Li, J. (2018). Satellite based atmospheric infrared sounder development and applications. *Bulletin of the American Meteorological Society*, 99(3), 583–603. <https://doi.org/10.1175/BAMS-D-16-0293.1>
- Mira, M., Valor, E., Boluda, R., Caselles, V., & Coll, C. (2007). Influence of soil water content on the thermal infrared emissivity of bare soils: Implication for land surface temperature determination. *Journal of Geophysical Research*, 112, F04003. <https://doi.org/10.1029/2007JF000749>
- Pavelin, E. G., & Candy, B. (2014). Assimilation of surface-sensitive infrared radiances over land: Estimation of land surface temperature and emissivity. *Quarterly Journal of the Royal Meteorological Society*, 140(681), 1198–1208. <https://doi.org/10.1002/qj.2218>
- Peres, L. F., & DaCamara, C. C. (2005). Emissivity maps to retrieve land-surface temperature from MSG/SEVIRI. *IEEE Transactions on Geoscience and Remote Sensing*, 43(8), 1834–1844. <https://doi.org/10.1109/TGRS.2005.851172>
- Salisbury, J. W., & D'Aria, D. M. (1992). Emissivity of terrestrial materials in the 8–14  $\mu\text{m}$  atmospheric window. *Remote Sensing of Environment*, 42(2), 83–106. [https://doi.org/10.1016/0034-4257\(92\)90092-X](https://doi.org/10.1016/0034-4257(92)90092-X)
- Saunders, R., Matricardi, M., & Brunel, P. (1999). An improved fast radiative transfer model for assimilation of satellite radiance observations. *Quarterly Journal of the Royal Meteorological Society*, 125(556), 1407–1425. <https://doi.org/10.1002/qj.1999.49712555615>
- Schmit, T. J., Griffith, P., Gunshor, M. M., Daniels, J. M., Goodman, S. J., & Lebar, W. J. (2017). A closer look at the ABI on the goes-r series. *Bulletin of the American Meteorological Society*, 98(4), 681–698. <https://doi.org/10.1175/BAMS-D-15-00230.1>
- Schmit, T. J., Gunshor, M. M., Menzel, W. P., Gurka, J. J., Li, J., & Bachmeier, A. S. (2005). Introducing the next-generation advanced baseline imager on GOES-R. *Bulletin of the American Meteorological Society*, 86(8), 1079–1096. <https://doi.org/10.1175/BAMS-86-8-1079>
- Seemann, S. W., Borbas, E. E., Knuteson, R. O., Stephenson, G. R., & Huang, H. L. (2008). Development of a global infrared land surface emissivity database for application to clear sky sounding retrievals from multispectral satellite radiance measurements. *Journal of Applied Meteorology and Climatology*, 47(1), 108–123. <https://doi.org/10.1175/2007JAMC1590.1>
- Skamarock, W. C., Klemp, J. B., Dudhia, J., Gill, D. O., Barker, D. M., Duda, M. G., et al. (2008). A description of the advanced research WRF version 3. *NCAR Tech. Note NCAR/TN-475+STR*.
- Snyder, W. C., Wan, Z., Zhang, Y., & Feng, Y. Z. (1998). Classification-based emissivity for land surface temperature measurement from space. *International Journal of Remote Sensing*, 19(14), 2753–2774. <https://doi.org/10.1080/014311698214497>
- Stokes, G. M., & Schwartz, S. E. (1994). The Atmospheric Radiation Measurement (ARM) program: Programmatic background and design of the cloud and radiation test bed. *Bulletin of the American Meteorological Society*, 75(7), 1201–1221. [https://doi.org/10.1175/1520-0477\(1994\)075%3C1201:TARMPP%3E2.0.CO;2](https://doi.org/10.1175/1520-0477(1994)075%3C1201:TARMPP%3E2.0.CO;2)
- Trigo, I. F., Boussetta, S., Viterbo, P., Balsamo, G., Beljaars, A., & Sandu, I. (2015). Comparison of model land skin temperature with remotely sensed estimates and assessment of surface-atmosphere coupling. *Journal of Geophysical Research: Atmospheres*, 120, 12,096–12,111. <https://doi.org/10.1002/2015JD023812>
- Wang, Z., & Sassen, K. (2001). Cloud type and macrophysical property retrieval using multiple remote sensors. *Journal of Applied Meteorology*, 40(10), 1665–1682. [https://doi.org/10.1175/1520-0450\(2001\)040%3C1665:CTAMPR%3E2.0.CO;2](https://doi.org/10.1175/1520-0450(2001)040%3C1665:CTAMPR%3E2.0.CO;2)
- Wu, X., & Smith, W. L. (1997). Emissivity of rough sea surface for 8–13  $\mu\text{m}$ : Modeling and verification. *Applied Optics*, 36(12), 2609–2619. <https://doi.org/10.1364/AO.36.002609>
- Xue, Y., & Forman, B. A. (2017). Atmospheric and forest decoupling of passive microwave brightness temperature observations over snow-covered terrain in North America. *IEEE Journal of Selected Topics in Applied Earth Observations and Remote Sensing*, 10(7), 3172–3189. <https://doi.org/10.1109/JSTARS.2016.2614158>
- Zhang, F., Minamide, M., & Clothiaux, E. E. (2016). Potential impacts of assimilating all-sky infrared satellite radiances from GOES-R on convection-permitting analysis and prediction of tropical cyclones. *Geophysical Research Letters*, 43, 2954–2963. <https://doi.org/10.1002/2016GL068468>

- Zheng, W., Wei, H., Wang, Z., Zeng, X., Meng, J., Ek, M., et al. (2012). Improvement of daytime land surface skin temperature over arid regions in the NCEP GFS model and its impact on satellite data assimilation. *Journal of Geophysical Research: Atmospheres*, *117*, D06117. <https://doi.org/10.1029/2011JD015901>
- Zhu, T., Weng, F., Masutani, M., & Woollen, J. S. (2012). Synthetic radiance simulation and evaluation for a joint observing system simulation experiment. *Journal of Geophysical Research: Atmospheres*, *117*, D23111. <https://doi.org/10.1029/2012JD017697>
- Zou, X., Zhuge, X., & Weng, F. (2016). Characterization of bias of Advanced Himawari Imager infrared observations from NWP background simulations using CRTM and RTTOV. *Journal of Atmospheric and Oceanic Technology*, *33*(12), 2553–2567. <https://doi.org/10.1175/JTECH-D-16-0105.1>